Exercise-stimulated muscle ROS production and glucose uptake requires NADPH oxidase 2

Carlos Henríquez-Olguin[1,2], Jonas R. Knudsen[1], Steffen H. Raun[1], Zhencheng Li[1], Emilie Dalbram[3], Jonas T. Treebak[3], Lykke Sylow[1], Rikard Holmdahl[4], Erik A. Richter[1], Enrique Jaimovich[2], and Thomas E. Jensen[1,*]

1. Department of Nutrition, Exercise and Sports, University of Copenhagen, Denmark
2. Center of Exercise, Metabolism and Cancer, Biomedical Sciences Institute, Universidad de Chile.
3. Novo Nordisk Foundation Center for Basic Metabolic Research, Research Program in Integrative Metabolism and Environmental Influence, Faculty of Health and Medical Sciences, University of Copenhagen, Denmark
4. Section for Medical Inflammation Research, Department of Medical Biochemistry and Biophysics, Karolinska Institute, Stockholm, Sweden.

* Corresponding author and person to who reprint requests should be addressed:

Thomas E. Jensen, PhD

Department of Nutrition, Exercise, and Sports (NEXS)

University of Copenhagen

Universitetsparken 13, DK-2100 Copenhagen, Denmark

Phone: +45 3532 1757

Email: TEJensen@NEXS.ku.dk

ABSTRACT

Reactive oxygen species (ROS) act as intracellular compartmentalized second messengers mediating metabolic stress-adaptation. In skeletal muscle fibers, ROS have been suggested to stimulate glucose transporter 4 (GLUT4)-dependent glucose transport during artificially evoked contraction *ex vivo* but whether myocellular ROS production is stimulated by *in vivo* exercise to control metabolism is unclear. Here, we combined exercise in humans and mice with fluorescent dyes, genetically-encoded biosensors, and NADPH oxidase 2 (NOX2) loss-of-function models to demonstrate that NOX2 is the main source of ROS during moderate-intensity exercise in skeletal muscle. Furthermore, two NOX2 loss-of-function mouse models lacking either p47phox or Rac1 presented striking phenotypic similarities, including greatly reduced exercise-stimulated glucose uptake and GLUT4 translocation. These findings indicate that NOX2 is a major myocellular ROS source regulating glucose transport capacity during moderate intensity exercise.

INTRODUCTION

A single bout of exercise prompts a rapid adaptive increase in energy substrate metabolism in contracting skeletal muscle to meet the increased demand for ATP production. Understanding the molecular signal transduction pathways, that orchestrate these metabolic responses in muscle has broad implications, from optimizing athletic performance, to understanding fundamental stress-adaptive responses at the cellular level, to prevention and treatment of aging- and lifestyle-related diseases in muscle and other tissues [1].

The production of oxygen-derived free radicals and derivatives thereof, collectively referred to as reactive oxygen species (ROS), increases in skeletal muscle during exercise and has long been considered to mediate adaptive responses to both acute bouts of exercise and chronic exercise training [2]. Although historically viewed as a by-product of oxidative metabolism in mitochondria, it has been suggested that ROS may be produced enzymatically by several potential sources in exercising muscle, including NADPH oxidase (NOX) and xanthine oxidase [3]. In contrast, mitochondria are likely not the major source of exercise-induced ROS [4, 5]. The major ROS source in the context of physiological *in vivo* exercise, however, remains uncertain due to the difficulty in measuring and quantifying exercise-stimulated ROS production [6].

Research in the past 60 years has established that glucose transport *in vivo* is controlled by a coordinated increase in glucose delivery, glucose transport into muscle fibers and intracellular metabolism [7, 8]. Among these events, the insulin-independent translocation of glucose transporter protein 4 (GLUT4) from intracellular storage depots to the cell surface to facilitate glucose entry appears to be a key molecular event [9, 10]. Studies in

isolated *ex vivo* incubated skeletal muscles from rodents have shown that glucose transport in response to electrically stimulated contraction and mechanical stress is lowered by antioxidants [11, 12], suggesting that ROS signal to increase glucose transport [13]. Interestingly, the small GTPase Rac1 is activated by muscle contraction and passive stretch and is necessary for both stimuli to increase glucose uptake in isolated mouse muscles [14, 15]. Rac1 is best known to bind and orchestrate regulators of actin remodeling[16], but the recruitment of GTP-loaded active Rac GTPase isoforms in conjunction with a complex of other NOX2 regulatory proteins (p67phox, p47phox and p40phox) is also essential to stimulate superoxide (O_2^-)-production by the membrane-bound NOX2 complex[17]. However, whether NOX2-induced ROS production regulates glucose uptake in vivo and if the reduced exercise-stimulated glucose uptake observed in Rac1 KO muscles[18] is due to reduced ROS production, is currently unknown.

In the present study, we took advantage of recent methodological approaches in the ROS signaling field, including a method for preservation of *in vivo* ROS modifications and genetically-encoded ROS biosensors [19]. This allowed us to measure both general and localized NOX2-specific ROS production in wild-type (WT) mice and mice lacking NOX2 activity due to the absence of either the Rac1 or p47phox regulatory subunits. Using these approaches, we show that NOX2 is activated by moderate intensity exercise and is the predominant source of ROS production under these conditions. Moreover, a large reduction in exercise-stimulated glucose uptake and GLUT4 translocation were shared features between the two NOX2 loss-of-function models. Collectively, these results imply that NOX2 is a major source of ROS production during moderate-intensity exercise and that Rac1 is required for GLUT4 translocation and glucose uptake due to its essential role in NOX2 activation.

RESULTS

Moderate intensity exercise increase ROS in human muscle

Plasma redox markers are increased during both moderate- and high-intensity exercise in humans[20]. However, whether muscle ROS production increases during moderate-intensity exercise in humans is unknown. To test this, we estimated total oxidant production in skeletal muscle from healthy young men before and after a single 30 min bout of bicycle ergometer exercise at a moderate 65% peak power output exercise intensity using the redox-sensitive dye dichlorodihydrofluorescein diacetate (DCF). We found that exercise stimulated a 86% increase in DCF oxidation in human skeletal muscle (Fig. 1A), which was accompanied by an expected increase in the phosphorylation state of known exercise-responsive proteins (Fig. 1B). This shows that moderate-intensity exercise increases ROS in human skeletal muscle.

ROS production during exercise requires NOX2 activity in mice

To dissect the ROS source during exercise, we used a previously described p47phox-mutated mice (*ncf1**) harboring a loss-of-function mutation in the regulatory NOX2 subunit, p47phox [21]. An acute moderate-intensity treadmill exercise bout (65% maximal running speed) for 20 min increased DCF oxidation (+ 45%) in WT mice, a response that was completely abolished in p47phox-deficient *ncf1** mice (Fig. 1C). This observation was found to be independent of alterations in antioxidant enzyme abundance in TA muscles from *ncf1** mice compared to WT mice (Fig. S1).

To substantiate that NOX2 activity was required for exercise-stimulated ROS production, we used inducible muscle-specific Rac1 knockout mice (Rac1 imKO), which are predicted to lack functional NOX2. Similar to the *ncf1** mice, exercise-stimulated DCF oxidation was completely absent in Rac1 imKO compared to WT

littermates (Fig. S-2C). To directly demonstrate NOX2 activation during *in vivo* exercise, we adapted a recently described redox histology method [19] that enabled the preservation and visualization of the redox state of a transfected oxidation-sensitive NOX2 activity reporter, p47-roGFP [22], in mouse muscle sections. In WT mice, electrical stimulation *in vitro* induced p47-roGFP oxidation in FDB fibers (Fig. S2B), as did treadmill exercise in TA muscle (Fig.1D). In contrast, exercise or electrical stimulation failed to increase p47-roGFP oxidation in Rac1 imKO. Importantly, the lack of response in Rac1 imKO mice occurred without changes in antioxidant enzymes abundance (Fig. S2B). Collectively, these results strongly suggest that NOX2 is activated and constitutes a source of ROS production during endurance-type exercise in skeletal muscle.

NOX2 is required for exercise-stimulated glucose uptake

Given that Rac1 imKO mice display a severe reduction in treadmill exercise-stimulated glucose uptake and GLUT4 translocation [18], we reasoned that if Rac1 was acting via NOX2 then *ncf1** mice should show a similar reduction. We first conducted a general characterization of *ncf1** mice. Similar total body weight but reduced fat mass was observed in *ncf1** mice compared to age-matched WT mice (Fig. S3). Respiratory exchange ratio (RER) was lower in *ncf1** mice during the light phase compared to WT mice (Fig. 2A), despite a similar habitual activity observed between genotypes (Fig. 2B). Thus, *ncf1** mice, similar to Rac1 imKO mice, display a shift towards fat oxidation at rest and during fasting.

Next, we determined whether NOX2-dependent ROS generation is required for exercise-stimulated glucose uptake. Each mouse was exercised at a relative work load corresponding to 65% of its maximum running capacity for 20 min. Exercise-induced 2-

[^{3}H] deoxyglucose (2DG) uptake was markedly attenuated in Quad, SOL and TA muscles from *ncf1** mice compared to WT (Fig. 2C-E). Importantly, the reduction of exercise-stimulated glucose uptake in *ncf1* mice* was not due to differences in maximal running capacity (Fig. 2F), blood glucose levels (Fig. 2G) or intramuscular energetics evaluated as NAD+ and NADH levels (Fig. 2H-I). However, plasma lactate levels were increased by exercise in WT but not in *ncf1** mice (Fig. 2J), consistent with a reduced reliance on glycolysis for energy production.

NOX2 is required for exercise-stimulated GLUT4 translocation

Next, we tested if the reduction in exercise-stimulated glucose uptake in *ncf1** mice could be explained by reduced GLUT4 translocation as seen in the Rac1 imKO [18]. Consistent with this notion, the exercise-stimulated increase in surface-membrane GLUT4-GFP-*myc* in TA muscle from WT was virtually abolished in *ncf1** mice (Fig. 3A). Importantly, total protein abundance of GLUT4 and HKII (Fig. 3B-D and Fig. S4) did not differ between genotypes nor did protein abundance of the mitochondrial electron transport chain complexes (Fig. 3E-F and Fig. S5). Taken together, these data demonstrate that *ncf1** mice phenocopy the Rac1 imKO mice in terms of pronounced impairments in exercise-stimulated muscle glucose uptake and GLUT4 translocation[18]. This strongly suggests that the common denominator between p47phox and Rac1, NOX2 activation, is required for exercise-stimulated glucose uptake and GLUT4 translocation.

Exercise-stimulated p38 MAPK$^{Thr180/Tyr182}$ phosphorylation is reduced in *ncf1 quadriceps muscle**

Exercise-induced ROS production has been suggested to activate a number of kinases linked to glucose uptake-regulation in skeletal muscle[23]. Interestingly, p-p38 MAPK$^{Thr180/Tyr182}$ levels were lower in quadriceps muscle of *ncf1** mice compared to WT mice after exercise, but not in soleus or TA muscles (Fig. 4). The phosphorylation of ERK $^{Thr202/Tyt204}$, AMPK^{Thr172}, and its substrate ACC^{Ser79} did not differ significantly between genotypes (Fig. 4) nor did total α2 AMPK, p38 MAPK, and ERK1/2 expression in any of the studied muscles (Fig. S6). Taken together, this makes reduced signaling by these kinases an unlikely explanation of the consistent reduction in exercise-stimulated glucose uptake in *ncf1** vs. WT mice across muscles.

DISCUSSION

The source of ROS during exercise and the role of ROS in the acute and chronic adaptations to exercise, in particular in the context of non-damaging moderate intensity *in vivo* exercise, has remained undetermined for more than 30 years [24]. The current study observed that moderate-intensity endurance exercise acutely increased ROS levels in both humans and mice. Strikingly, functional NOX2 was required for the exercise-stimulated ROS increase and is thus a major source of ROS during moderate intensity exercise. Furthermore, NOX2 activity was a major requirement for exercise-stimulated GLUT4 translocation and glucose uptake in skeletal muscle, providing a likely molecular explanation of why Rac1 imKO mice have a strong impairment of exercise-stimulated GLUT4 translocation and glucose uptake.

We and others have shown that the small rho family GTPase Rac1 is necessary for insulin-stimulated, muscle-contraction and passive stretch-induced skeletal muscle glucose uptake [14, 15, 25]. We have previously found this Rac1-dependency of glucose uptake and GLUT4 translocation to be more pronounced during *in vivo* treadmill

exercise compared to in vitro contractions [18]. The GLUT4 trafficking field has mostly focused on Rac1 as an orchestrator of the dynamic reorganization of the cortical actin cytoskeleton consisting of the cytoplasmic β and γ actin-isoforms [16]. This actin-reorganization was shown to be crucial for insulin-stimulated GLUT4 translocation in muscle cells [26]. However, the cytoplasmic β and γ actin-isoforms are both downregulated during muscle differentiation and whether dynamic reorganization occurs in adult skeletal muscle fibers similarly to in cells is presently unclear [27]. Our present data suggest that NOX2 is a vital downstream mediator of the effect of Rac1 on exercise-induced glucose uptake and GLUT4 translocation since the Rac1 imKO phenotype is shared by mice lacking another essential regulatory subunit of NOX2, p47phox. In addition, our *in vivo* glucose uptake data provide a likely physiological mechanism explaining why exogenous antioxidants inhibit *ex vivo* contraction- and stretch-stimulated glucose uptake [11, 12]. The relative dependence on actin and NOX2 and whether NOX2 and actin interact in muscle to regulate glucose uptake, as suggested in other cell types[28], should be clarified in future studies.

Due to the uncertainties regarding the downstream events mediating NOX2 signal transduction, we utilized a classical, non-ROS-specific redox-sensitive fluorescent DCF which, upon oxidation, is converted into fluorescent DCF [29]. DCF fluorescence should thus be regarded as a general measure of total cellular oxidant levels rather than a specific measure of a particular ROS[30]. We observed an increase in DCF fluorescence in exercising mice and humans. Remarkably, despite the non-specific nature of DCF oxidation, we found that the increase in exercise-stimulated DCF fluorescence was virtually abolished in mice lacking either Rac1 or p47phox components of NOX2. Regardless of the exact ROS measured, this indicates that NOX2 is a predominant source of ROS in skeletal muscle of exercising mice.

In the current study, the exercise-stimulated phosphorylation of p-p38MAPK was reduced in *ncf1** mice compared to WT, in particular in quadriceps muscle. As p38 MAPK has been proposed as a regulator of muscular glucose uptake [12], we cannot exclude that reduced p38 MAPK contributed to the reduced glucose uptake we observed in *ncf1** mice. However, the reduction in exercise-stimulated kinase signaling is less consistent than the reduction in glucose uptake in the different muscles analyzed in the *ncf1** mice. Moreover, Rac1 imKO mice share the same glucose uptake phenotype without showing reductions in stretch-stimulated signaling, including p38 MAPK[18]. Instead, we speculate that the shared reduction in exercise-stimulated glucose uptake in *ncf1** and Rac1 imKO mice might relate to a shared and yet undetermined redox-sensitive signaling mechanism. Worth noting, we believe NOX2 to signal independently of the AMPK-TBC1D1 signaling axis, based on the previous work by us and others [14, 31, 32, 33, 34]. Future studies should work to identify the shared cell signaling traits between different NOX2-deficient mouse models using e.g. redox proteomics [35].

In conclusion, this study showed for the first time that NOX2 is activated during moderate-intensity exercise in human and mouse skeletal muscle and is a major source of ROS under such conditions. Furthermore, our comparison of two mouse models lacking regulatory NOX2 subunits showed that lack of ROS generation during exercise strongly impaired muscle glucose uptake and GLUT4 translocation during exercise. This indicates that NOX2 is a major source of ROS generation during exercise and that NOX2-dependent ROS production is an important signal for increasing muscle glucose uptake during exercise.

MATERIAL AND METHODS

Animals. All experiments were approved by the Danish Animal Experimental Inspectorate (2015−15−0201−00477). Inducible muscle-specific male Rac1 mice (imKO) and littermate control mice were generated by crossbreeding $Rac1^{fl/fl}$ mice [36] with mice expressing Cre recombinase from a tetracycline-controlled transactivator coupled to the human skeletal actin promoter [37]. For muscle-specific Rac1 deletion, all mice were treated with doxycycline in the drinking water around 10-14 weeks of age (1g/L; Sigma Aldrich) for 3 weeks followed by a wash out period of 3 weeks.

Male B10.Q wild-type (WT) and B10.Q. p47phox mutated (*ncf1**) mice contain a point mutation in exon 8 [21]. All mice were group-housed maintained on a 12:12-h light-dark cycle, at 21º C, and received standard rodent chow diet (Altromin no. 1324; Chr. Pedersen, Denmark) and water ad libitum.

In vivo gene transfer in adult skeletal muscle. For the *in vivo* transfection experiments, mice were anesthetized with 2-3% isoflurane. Hyaluronidase (Sigma-Aldrich) dissolved in sterile saline solution (0.36 mg/ml) was injected subcutaneously in FDB and intramuscularly in TA muscle, followed by 20 and 40 µg plasmid injections 1 hour later, respectively. FDB muscle electroporation was performed by delivering 10 electrical pulses at an intensity of 75 V/cm, 10-ms pulse duration, 200-ms pulse interval using acupuncture needles (0.20 x 25 mm, Tai Chi, Lhasa OMS) connected to an ECM 830 BTX electroporator (BTX Harvard Apparatus). TA electroporation was performed following the same protocol but raising the intensity to 100 V/cm (#45-0101 Caliper Electrode, BTX Caliper Electrodes, USA). The p47-roGFP construct used to determine NOX2 activity was a kind gift from Dr. George G. Rodney [22]. The GLUT4-myc-GFP construct was a kind gift from Dr. Jonathan Bogan (Addgene plasmid # 52872).

Metabolic Chambers. O_2 uptake (VO_2) and CO_2 production (VCO_2) were measured using a CaloSys apparatus (TSE Systems, Bad Homburg, Germany). The data presented is the average for light and dark periods measured over 2 consecutive days in WT and *ncf1** mice. The respiratory exchange ratio (RER) was calculated as VCO_2 production/VO_2 uptake.

Maximal running tests. Mice were acclimated to the treadmill three times (15 min at 0.16 m/s) (Treadmill TSE Systems) a week prior to the maximal running tests. The maximal running test started at 0.16 m/s for 300 s with 10 % incline, followed by a continuing increase (0.2 m/s) in running speed every 60s until exhaustion. Exhaustion was defined as the point at which instead of running on the treadmill, the mice fall back on the grid 3 times within a 30 sec period. Maximal running speed was determined as the last completed stage during the incremental test.

FDB fiber isolation. Muscle fibers were obtained by enzyme digestion of the whole muscle with collagenase type II (1.5 mg/ml) (Worthington, Lakewood, NJ) for 90 min at 37°C followed by mechanical dissociation with fire polished Pasteur pipettes. Isolated fibers were seeded in ECM Gel-coated (Sigma-Aldrich) cell culture dishes in DMEM supplemented with 10% fetal bovine serum. After 16 h of seeding, the fibers were used for experimentation. Electrical stimulation protocol (10 V, 1 Hz, 0.1 ms duration) was delivered to isolated FDBs for 15 min via field electric field stimulation device (RC-37FS, Warner instruments, USA).

Redox changes in muscle cryosections. TA muscles were dissected and embedded in optimum cutting temperature (OCT) medium from Tissue Tek, frozen in melting

isopentane and kept at -80 °C until processing. Total oxidant levels were estimated as previously described [13]. Briefly, 10 μm thickness muscle cryosections were incubated with 5 μM of 2',7'-dichlorodihydrofluorescein diacetate (DCF; Molecular Probes, Eugene) and allowed to dry overnight at room temperature in dark. Muscle membranes were visualized using Texas red□labeled wheat germ agglutinin (WGA; Molecular Probes). The redox histology was performed as previously described [19]. p47roGFP-transfected muscle cryosections were incubated with PBS containing 50 mM N-Ethylmaleimide (NEM) for 10 min at 4°C, followed by fixation using 4% paraformaldehyde for 10 min at room temperature.

Running-stimulated muscle 2-deoxyglucose (DG) uptake. Muscle-specific 2DG uptake was measured as previously described[31]. [^{3}H]2DG (PerkinElmer) was injected intraperitoneally (as a bolus in saline, 10 μL/g body weight) containing 0.1 mmol/L 2DG and 50 μCi/mL [^{3}H]2DG corresponding to ∼12 μCi/mouse) into fed mice immediately before the exercise bout. Blood glucose was measured before and immediately after 20 min of exercise. Mice were euthanized by cervical dislocation, and muscle tissues and plasma samples quickly frozen in liquid nitrogen and stored at −80°C until analysis. Samples were deproteinated using 0.1 mol/L Ba $(OH)_2$ and 0.1 mol/L $ZnSO_4$. The total muscle [^{3}H]2DG tracer activity found in 2DG-6-phosphate was divided by the area under the curve of the specific activity at time points 0 and 20 min multiplied with the average blood glucose at time points 0 and 20 min. This was related to muscle weight and the time to obtain the tissue-specific 2DG uptake as micromoles per gram per hour.

In vivo GLUT4 translocation. Immediately after exercise, TA muscles were fixed by immersion in ice-cold 4% in paraformaldehyde in PBS for 4 h. Individual fibers were

324 teased from fixed muscle with fine forceps under a dissection microscope. Non-
325 permeabilized isolated muscle fibers were incubated in 1% BSA in PBS for 1 h min and
326 then incubated with an anti-myc antibody (rabbit polyclonal) overnight (CST, #2278).
327 The next day fibers were incubated with a secondary antibody conjugated with Alexa
328 Fluor 568 (Invitrogen, UK). The muscle fibers were mounted in Vectashield mounting
329 medium.

330 ***Western blot analyses.*** Tissue was homogenized for 1 min at 30 Hz using a Tissue
331 Lyser in ice cold lysis buffer (0.05 mol/L Tris Base pH 7.4, 0.15 mol/L NaCl, 1 mmol/
332 L EDTA and EGTA, 0.05mol/L sodium flouride, 5 mmol/L sodium pyrophosphate, 2
333 mmol/L sodium orthovanadate, 1 mmol/L benzamidine, 0.5% protease inhibitor
334 cocktail (P8340, Sigma Aldrich), and 1% NP- 40). After rotating end-over-end for 30
335 min, lysate supernatants were collected by centrifugation (18,327 g) for 20 min at 4°C.
336 Lysate protein concentrations were determined using BSA standards and bicinchoninic
337 acid assay reagents (Pierce). Total protein and phosphorylation levels of relevant
338 proteins were determined by standard immunoblotting techniques, loading equal
339 amounts of protein. The primary antibodies used p-AMPK^{Thr172} (Cell Signaling
340 Technology (CST)), #2535S), p-p38 MAPK$^{Thr180/Tyr182}$ (CST, #9211), Hexokinase II
341 (CST, #2867), GLUT4 p-ACC2 Ser^{212} (Millipore, 03-303), (ThermoFisher Scientific,
342 PA-23052), Rac1 (BD Biosciences, #610650), NOX2 (Abcam, #Ab129068), Catalase
343 (SCBT, sc-271803), MnSOD (Millipore, 06-984), TRX2 (SCBT, sc-50336), actin
344 (CST, #4973) total p38 MAPK (CST, #9212), alpha2 AMPK (a gift from D. Grahame
345 Hardie, University of Dundee), total ERK 1/2 (CST, #9102), and TBC1D1^{ser231}
346 (Millipore #07-2268), OXPHOS cocktail (Abcam, #ab110413) and Hexokinase II
347 (CST, #2867). All antibodies were optimized for signal linearity. Membranes were
348 blocked for 1 h at room temperature in TBS-Tween 20 containing either 2% skimmed

milk or 2% BSA and incubated overnight at 4°C with primary antibody. The membranes were incubated in the corresponding horseradish peroxidase-conjugated secondary antibody for 1 h at room temperature and washed in TBST before visualization of the proteins (ChemiDoc^{TM}MP Imaging System, Bio Rad).

Imaging and imaging analysis. For all live-imaging experiments confocal images were collected using a 63x 1.4 NA oil immersion objective lens on an LSM 780 confocal microscope (Zeiss) driven by Zen 2011. FDB fibers were imaged in phenol red-free growth medium (5 % horse serum) while kept at 95 % O_2 and 5 % CO_2 and 37°C using a Pecon Lab-Tek S1 heat stage.

Human experiments. Three young (Age 29 ± 3.56y BMI 24.8 ± 1.76 kg/m^2), healthy men gave their written, informed consent to participate in the study approved by the Regional Ethics Committee for Copenhagen (H-16040740) and complied with the ethical guidelines of the Declaration of Helsinki II. The volunteers visited the laboratory on two separate days. The first day, the subjects completed an incremental test on a Monark Ergomedic 839E cycle ergometer (Monark, Sweden) to determine peak power output (PPO). On the second day, each subject performed a 30-min exercise trial at the intensity corresponding to ~65% of their individual PPO in fasted state. Muscle biopsies were obtained from the m. vastus lateralis under local anesthesia [~3ml xylocaine (20mg ml−1lidocaine), Astra, Stockholm, Sweden] before and after exercise using a 5 mm Bergstrom needle with suction. The muscle biopsies were embedded in optimal cutting temperature compound (tissue-tek) and frozen in liquid nitrogen-cooled isopentane and stored at −80°C for further analysis.

Statistical analyses. Results are shown as individual values or means ± S.E.M. Statistical testing was carried out using *t*-tests or two-way (repeated measures when appropriate) ANOVA as applicable. Tukey's *post hoc* test was performed to pinpoint significant differences between groups. Statistical analyses were performed using GraphPad Prism.

Acknowledgements. ZL was supported by Chinese Scholarship Council PhD stipends. LS was supported by a Danish Research Council grant 4004-00233 and Novo Nordisk Foundation Excellence grant NNF18OC0032082. CHO was supported by a CONICYT PhD travel grant. JRK was supported by Danish Diabetes Academy PhD stipends. EJ was supported by FONDECYT grant 1151293. TEJ was supported by a Novo Nordisk Foundation Excellence project grant (#15182). EAR was supported by the Danish Council for Independent Research/Science 6108-00203. We thank Kim Anker Sjøberg for pre-testing the human subjects and Betina Bolmgren for technical assistance with measuring 2DG uptake. Imaging data were collected at the Center for Advanced Bioimaging and the Core Facility for Integrated Microscopy, University of Copenhagen, Denmark.

Author Contribution. Conceptualization, CHO, EJ and TEJ. Methodology, CHO and TEJ. Investigation, CHO, JRK, ZL, ED, JTT, SHR, RH, EAR and LS. Formal analysis, CHO. Visualization, CHO. Writing – Original draft, CHO and TEJ. Writing – Review and Editing, CHO with input from all authors. Funding Acquisition, TEJ. Supervision, EJ and TEJ.

REFERENCES

1. Egan B, Zierath JR. Exercise metabolism and the molecular regulation of skeletal muscle adaptation. *Cell metabolism* **17**, 162-184 (2013).

2. Powers SK, Jackson MJ. Exercise-induced oxidative stress: cellular mechanisms and impact on muscle force production. *Physiol Rev* **88**, 1243-1276 (2008).

3. Powers SK, Radak Z, Ji LL. Exercise-induced oxidative stress: past, present and future. *J Physiol* **594**, 5081-5092 (2016).

4. Sakellariou GK*, et al.* Studies of mitochondrial and nonmitochondrial sources implicate nicotinamide adenine dinucleotide phosphate oxidase(s) in the increased skeletal muscle superoxide generation that occurs during contractile activity. *Antioxidants & redox signaling* **18**, 603-621 (2013).

5. Michaelson LP, Shi G, Ward CW, Rodney GG. Mitochondrial redox potential during contraction in single intact muscle fibers. *Muscle Nerve* **42**, 522-529 (2010).

6. Jackson MJ. Recent advances and long-standing problems in detecting oxidative damage and reactive oxygen species in skeletal muscle. *J Physiol* **594**, 5185-5193 (2016).

7. Richter EA, Hargreaves M. Exercise, GLUT4, and skeletal muscle glucose uptake. *Physiol Rev* **93**, 993-1017 (2013).

8. Sylow L, Kleinert M, Richter EA, Jensen TE. Exercise-stimulated glucose uptake - regulation and implications for glycaemic control. *Nat Rev Endocrinol* **13**, 133-148 (2017).

9. Kristiansen S, Hargreaves M, Richter EA. Exercise-induced increase in glucose transport, GLUT-4, and VAMP-2 in plasma membrane from human muscle. *Am J Physiol* **270**, E197-201 (1996).

10. Zisman A*, et al.* Targeted disruption of the glucose transporter 4 selectively in muscle causes insulin resistance and glucose intolerance. *Nat Med* **6**, 924-928 (2000).

11. Sandstrom ME*, et al.* Role of reactive oxygen species in contraction-mediated glucose transport in mouse skeletal muscle. *J Physiol* **575**, 251-262 (2006).

12. Chambers MA, Moylan JS, Smith JD, Goodyear LJ, Reid MB. Stretch-stimulated glucose uptake in skeletal muscle is mediated by reactive oxygen species and p38 MAP-kinase. *J Physiol* **587**, 3363-3373 (2009).

13. Merry TL, Steinberg GR, Lynch GS, McConell GK. Skeletal muscle glucose uptake during contraction is regulated by nitric oxide and ROS independently of AMPK. *Am J Physiol Endocrinol Metab* **298**, E577-585 (2010).

14. Sylow L, *et al.* Rac1 is a novel regulator of contraction-stimulated glucose uptake in skeletal muscle. *Diabetes* **62**, 1139-1151 (2013).

15. Sylow L, Moller LL, Kleinert M, Richter EA, Jensen TE. Stretch-stimulated glucose transport in skeletal muscle is regulated by Rac1. *J Physiol* **593**, 645-656 (2015).

16. Chiu TT, Jensen TE, Sylow L, Richter EA, Klip A. Rac1 signalling towards GLUT4/glucose uptake in skeletal muscle. *Cell Signal* **23**, 1546-1554 (2011).

17. Bedard K, Krause KH. The NOX family of ROS-generating NADPH oxidases: physiology and pathophysiology. *Physiol Rev* **87**, 245-313 (2007).

18. Sylow L, *et al.* Rac1 governs exercise-stimulated glucose uptake in skeletal muscle through regulation of GLUT4 translocation in mice. *J Physiol* **594**, 4997-5008 (2016).

19. Fujikawa Y, *et al.* Mouse redox histology using genetically encoded probes. *Science signaling* **9**, rs1 (2016).

20. Margaritelis NV, *et al.* Adaptations to endurance training depend on exercise-induced oxidative stress: exploiting redox interindividual variability. *Acta physiologica (Oxford, England)* **222**, (2018).

21. Hultqvist M, Olofsson P, Holmberg J, Backstrom BT, Tordsson J, Holmdahl R. Enhanced autoimmunity, arthritis, and encephalomyelitis in mice with a reduced oxidative burst due to a mutation in the Ncf1 gene. *Proceedings of the National Academy of Sciences of the United States of America* **101**, 12646-12651 (2004).

22. Pal R, Basu Thakur P, Li S, Minard C, Rodney GG. Real-time imaging of NADPH oxidase activity in living cells using a novel fluorescent protein reporter. *PLoS One* **8**, e63989 (2013).

23. Ji LL, Kang C, Zhang Y. Exercise-induced hormesis and skeletal muscle health. *Free radical biology & medicine* **98**, 113-122 (2016).

24. Davies KJ, Quintanilha AT, Brooks GA, Packer L. Free radicals and tissue damage produced by exercise. *Biochem Biophys Res Commun* **107**, 1198-1205 (1982).

25. Ueda S, *et al.* Crucial role of the small GTPase Rac1 in insulin-stimulated translocation of glucose transporter 4 to the mouse skeletal muscle sarcolemma. *FASEB journal : official publication of the Federation of American Societies for Experimental Biology* **24**, 2254-2261 (2010).

26. Chiu TT, Patel N, Shaw AE, Bamburg JR, Klip A. Arp2/3- and cofilin-coordinated actin dynamics is required for insulin-mediated GLUT4 translocation to the surface of muscle cells. *Mol Biol Cell* **21**, 3529-3539 (2010).

27. Madsen AB, *et al.* beta-actin shows limited mobility and is only required for supraphysiological insulin-stimulated glucose transport in young adult soleus muscle. *Am J Physiol Endocrinol Metab*, (2018).

28. Wilson C, *et al.* A Feed-Forward Mechanism Involving the NOX Complex and RyR-Mediated Ca2+ Release During Axonal Specification. *J Neurosci* **36**, 11107-11119 (2016).

29. Keller A, Mohamed A, Drose S, Brandt U, Fleming I, Brandes RP. Analysis of dichlorodihydrofluorescein and dihydrocalcein as probes for the detection of intracellular reactive oxygen species. *Free Radic Res* **38**, 1257-1267 (2004).

30. Chen X, Zhong Z, Xu Z, Chen L, Wang Y. 2',7'-Dichlorodihydrofluorescein as a fluorescent probe for reactive oxygen species measurement: Forty years of application and controversy. *Free Radic Res* **44**, 587-604 (2010).

31. Sylow L, *et al.* Rac1 and AMPK Account for the Majority of Muscle Glucose Uptake Stimulated by Ex Vivo Contraction but Not In Vivo Exercise. *Diabetes* **66**, 1548-1559 (2017).

32. Jensen TE, *et al.* Contraction-stimulated glucose transport in muscle is controlled by AMPK and mechanical stress but not sarcoplasmatic reticulum Ca(2+) release. *Mol Metab* **3**, 742-753 (2014).

33. Dokas J, *et al.* Conventional knockout of Tbc1d1 in mice impairs insulin- and AICAR-stimulated glucose uptake in skeletal muscle. *Endocrinology* **154**, 3502-3514 (2013).

34. Szekeres F, *et al.* The Rab-GTPase-activating protein TBC1D1 regulates skeletal muscle glucose metabolism. *Am J Physiol Endocrinol Metab* **303**, E524-533 (2012).

35. McDonagh B, Sakellariou GK, Jackson MJ. Application of redox proteomics to skeletal muscle aging and exercise. *Biochem Soc Trans* **42**, 965-970 (2014).

36. Chrostek A, *et al.* Rac1 is crucial for hair follicle integrity but is not essential for maintenance of the epidermis. *Molecular and cellular biology* **26**, 6957-6970 (2006).

37. Rao P, Monks DA. A tetracycline-inducible and skeletal muscle-specific Cre recombinase transgenic mouse. *Dev Neurobiol* **69**, 401-406 (2009).

FIGURE LEGENDS

Figure 1. Moderate-intensity exercise increases ROS production in a NOX2-dependent manner. A) Dichlorofluorescein (DCF) oxidation and B) exercise signaling

in muscle biopsies before and after a bout of moderate-intensity cycling (30 min, 65% maximal power output) in young-healthy volunteers (n=3). C) Representative images and quantification of the exercise-stimulated (20 min, 65% maximal running speed) DCF oxidation in tibialis anterior (TA) muscle from WT and *ncf1** mice (n=5). D) Representative image and quantification of the *in vivo* running-induced p47roGFP oxidation in tibialis anterior (TA) muscle in WT and Rac1 imKO mice. Scale bar=50 uM. For A) Unpaired t-test was performed for statistical analysis, * denotes P< 0.05 compared to resting condition. For C-D) Two-way ANOVA was performed to test for effects of exercise (exer) genotype (geno), and interaction (Int), followed by Tukey's *post hoc* corrected for multiple comparisons. #, ### denotes P< 0.05 and p< 0.001, respectively compared to the WT group. Values are mean ± SEM.

Figure 2. Exercise-stimulated glucose uptake is reduced in *ncf1 mice**. Different parameters were compared between p47phox mutated mice (*ncf1**) and wild-type (WT) mice. A) Respiratory exchange ratio (RER) during light and dark cycle and B) habitual activity. C-E) *In vivo* running-induced (20 min, 65% maximal running speed) 2-deoxy-glucose uptake (2DG) uptake in WT and *ncf1** mice (n=12-16). F) Maximal running speed (n=15 per group), G) blood glucose concentration after rest/exercise (n=6-8), H) NAD+, I) NADPH levels in quadriceps muscle (n=6-8), and J) Plasma lactate concentration. Unpaired t-test (F) and two-way ANOVA were performed to test for effects of exercise (Exer) genotype (Geno), and interaction (Int), followed by a Tukey's *post hoc* corrected for multiple comparisons. Data is shown as mean and SEM. #, ### denotes P< 0.05 and p< 0.001, respectively compared to the WT group (n=8 per group).

Figure 3. Exercise-stimulated GLUT4 translocation requires p47phox. A) The GLUT4-myc-GFP construct was electroporated into tibialis anterior (TA) muscles of both WT and *ncf1** mice. Non-permeabilized muscle fibers from exercised (20 min, 65% maximal running speed) or resting mice were stained with anti-*myc* antibody and imaged by confocal microscopy (n=3-5). Total endogenous GLUT4 and HK II were determined by western blot in the following muscles B) quadriceps, C) soleus, and D) TA muscles in WT and *ncf1** mice (n=14). Total oxphos proteins were determined in E) quadriceps and F) Soleus muscle. Unpaired t-test (B-D) and two-way ANOVA were performed to test for effects of exercise (Exer) genotype (Geno), and interaction (Int), followed by a Tukey's *post hoc* corrected for multiple comparisons. Values are mean ± SEM.

Figure 4. Exercise-stimulated intracellular signaling in *ncf1 muscles.** Activation of intracellular kinases after moderate-intensity treadmill exercise (20 min, 65% maximal running speed) in muscle lysates of A) quadriceps, B) Soleus, and C) tibialis anterior from WT and p47phox-mutated (*ncf1**) mice (n=6-8). Two-way ANOVAs was performed to test for effects of exercise (Exer) genotype (Geno), and interaction (Int), followed by Tukey's *post hoc* corrected for multiple comparisons. # denotes $P< 0.05$ compared to the WT group. Values are mean ± SEM.

Figure S1. Similar abundance of antioxidant enzymes in *ncf1 muscles.** *Tibialis anterior* muscle lysates from both *ncf1** and WT mice. Values are mean ± SEM.

Figure S2. Rac1 imKO mice fail to increase ROS production *in vitro* and *in vivo*. A) ROS generation induced by electrical stimulation in FDB Rac1 imKO fibers (*n*=5) b)

redox-regulated proteins in FDB fibers are similar between WT and Rac1 imKO muscle (*n*=5). C) DCF oxidation after 20 min of exercise in WT and Rac1 imKO *tibialis anterior* muscle (*n*=4). Two-way ANOVA were performed to test for effects of exercise (Exer) genotype (Geno), and interaction (Int), followed by a Tukey's *post hoc* corrected for multiple comparisons. # denotes P< 0.05 respectively compared to the WT group. Values are mean ± SEM.

Figure S3. Body weight and composition of *ncf1 mice.** a) Similar body weight despite tendency to b) lower body fat and c) higher lean mass and d) equal oxygen consumption in *ncf1** compared to WT mice. The midline represents the median; box represents the IQR between the first and third quartiles, and whiskers represent the lowest or highest values within 1.5 times IQR from the first or third quartiles. Unpaired t-test (F) and two-way ANOVA were performed to test for effects of exercise (Exer) genotype (Geno), and interaction (Int), followed by a Tukey's *post hoc* corrected for

Figure S4. Similar endogenous glucose handling-related protein abundance in *nfc1 and WT muscles.** Quantification of protein levels showed in figure 3B-D in a) quadriceps b) soleus, and c) *tibialis anterior* muscle. Values are mean ± SEM.

Figure S5. Oxphos protein content in *ncf1 muscles are similar to WT.** Quantification of protein levels showed in figure 3E-F in a) quadriceps and b) soleus muscle. Values are mean ± SEM.

Figure S6. Total AMPK, p38 MAPK and ERK protein in *ncf1 muscles.** Quantification of protein levels showed in figure 4A-C in a) quadriceps and b) soleus and *tibialis anterior* muscle. Values are mean ± SEM.

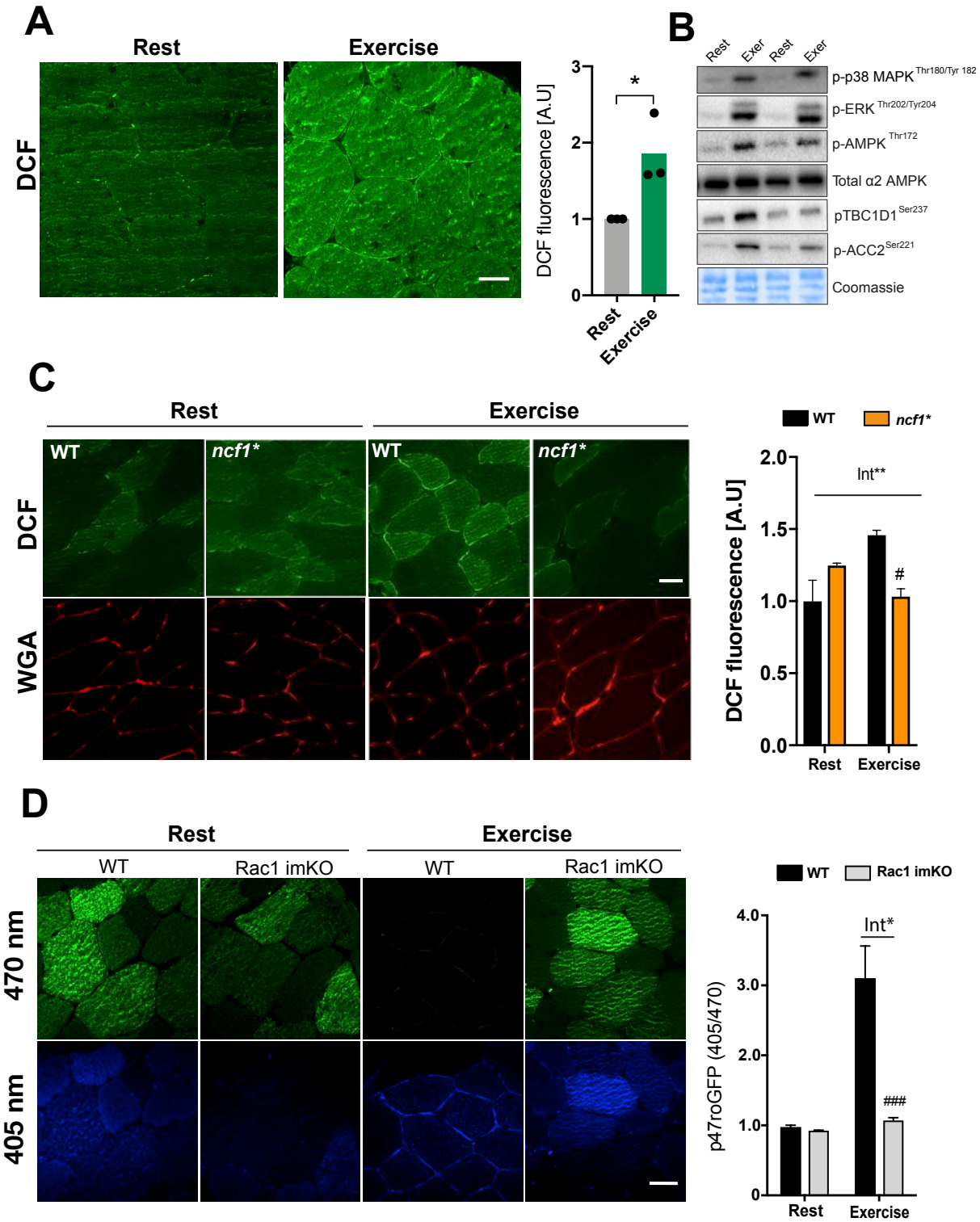
A
Rest
Exercise
DCF
DCF fluorescence [A.U]
3
2
1
0
*
Rest
Exercise
B
Rest
Exer
Rest
Exer
p-p38 MAPK Thr180/Tyr 182
p-ERK Thr202/Tyr204
p-AMPK Thr172
Total α2 AMPK
pTBC1D1 Ser237
p-ACC2 Ser221
Coomassie
C
Rest
Exercise
WT
ncf1*
WT
ncf1*
DCF
WGA
WT
ncf1*
DCF fluorescence [A.U]
2.0
1.5
1.0
0.5
0.0
Int**
#
Rest
Exercise
D
Rest
Exercise
WT
Rac1 imKO
WT
Rac1 imKO
470 nm
405 nm
WT
Rac1 imKO
p47roGFP (405/470)
4.0
3.0
2.0
1.0
0
Int*
###
Rest
Exercise

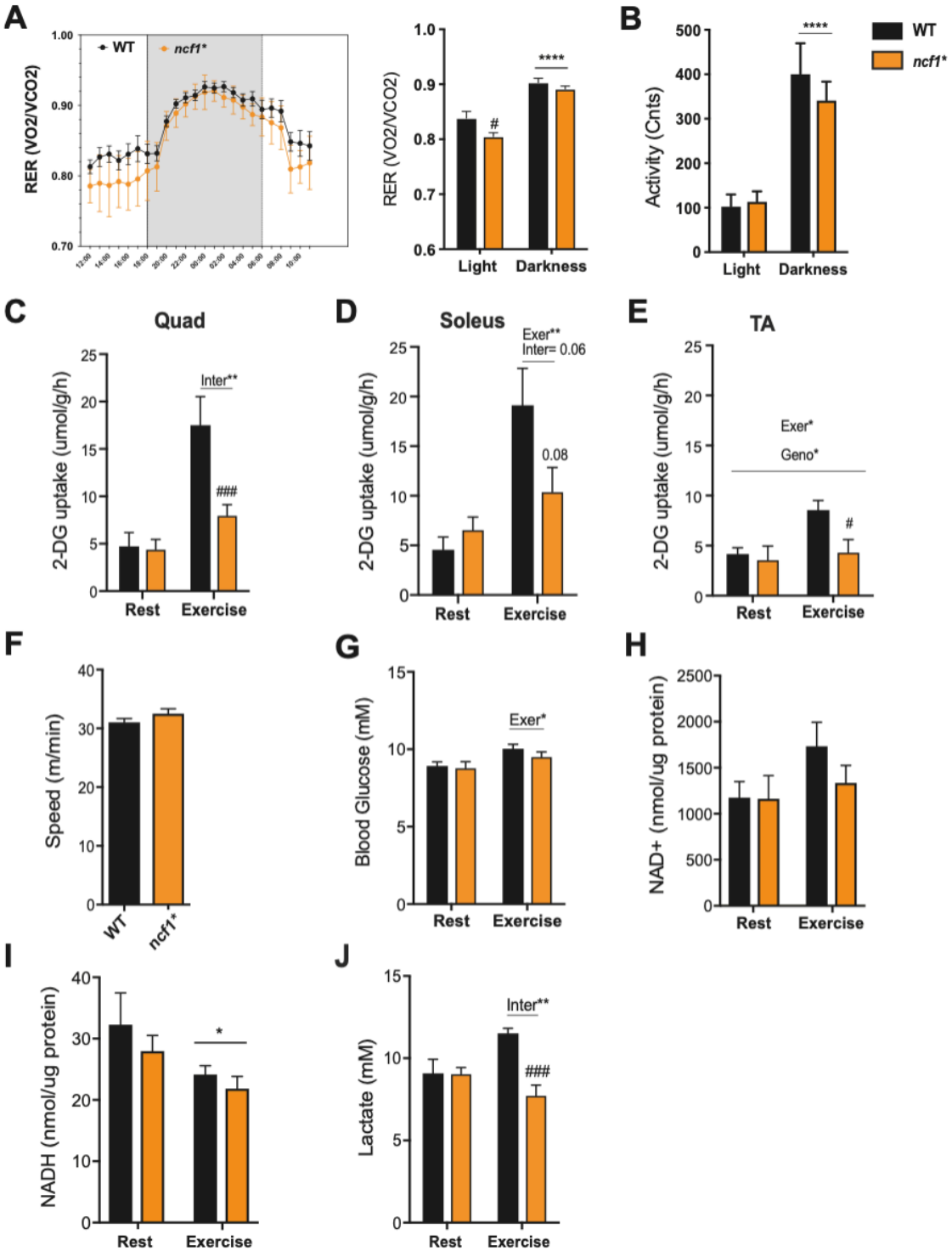
A
WT
ncf1*
RER (VO2/VCO2)
1.00
0.90
0.80
0.70
RER (VO2/VCO2)
1.0
0.9
0.8
0.7
0.6
#
****
Light
Darkness
B
WT
ncf1*
Activity (Cnts)
500
400
300
200
100
0
****
Light
Darkness
C
Quad
2-DG uptake (umol/g/h)
Inter**
###
Rest
Exercise
D
Soleus
2-DG uptake (umol/g/h)
Exer**
Inter= 0.06
0.08
Rest
Exercise
E
TA
2-DG uptake (umol/g/h)
Exer*
Geno*
#
Rest
Exercise
F
Speed (m/min)
WT
ncf1*
G
Blood Glucose (mM)
Exer*
Rest
Exercise
H
NAD+ (nmol/ug protein)
2500
2000
1500
1000
500
0
Rest
Exercise
I
NADH (nmol/ug protein)
*
Rest
Exercise
J
Lactate (mM)
Inter**
###
Rest
Exercise

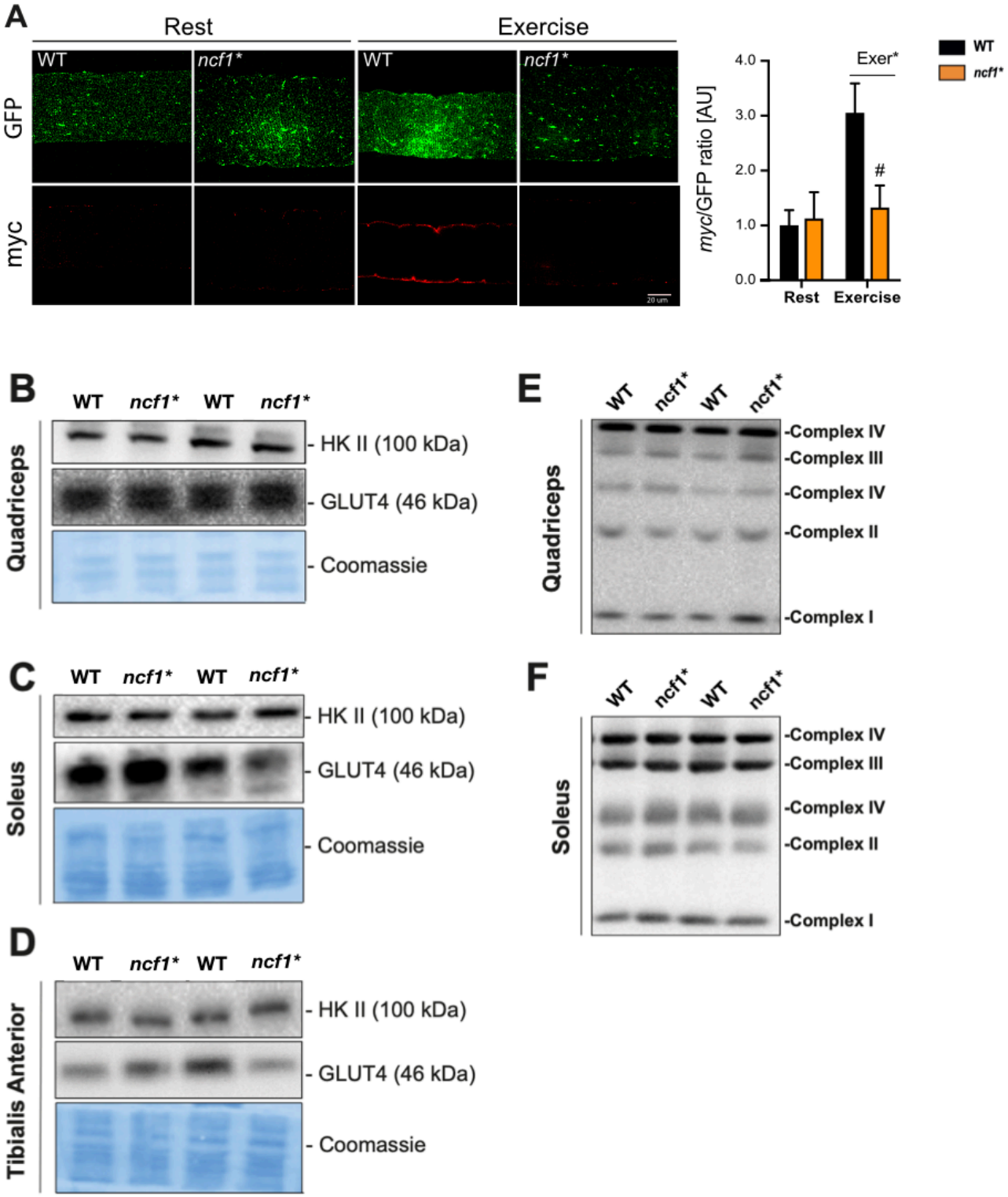
A
Rest
Exercise
WT
ncf1*
WT
ncf1*
GFP
myc
20 um
Exer*
#
myc/GFP ratio [AU]
4.0
3.0
2.0
1.0
0.0
Rest
Exercise
WT
ncf1*
B
WT
ncf1*
WT
ncf1*
Quadriceps
- HK II (100 kDa)
- GLUT4 (46 kDa)
- Coomassie
C
WT
ncf1*
WT
ncf1*
Soleus
- HK II (100 kDa)
- GLUT4 (46 kDa)
- Coomassie
D
WT
ncf1*
WT
ncf1*
Tibialis Anterior
- HK II (100 kDa)
- GLUT4 (46 kDa)
- Coomassie
E
WT
ncf1*
WT
ncf1*
Quadriceps
-Complex IV
-Complex III
-Complex IV
-Complex II
-Complex I
F
WT
ncf1*
WT
ncf1*
Soleus
-Complex IV
-Complex III
-Complex IV
-Complex II
-Complex I

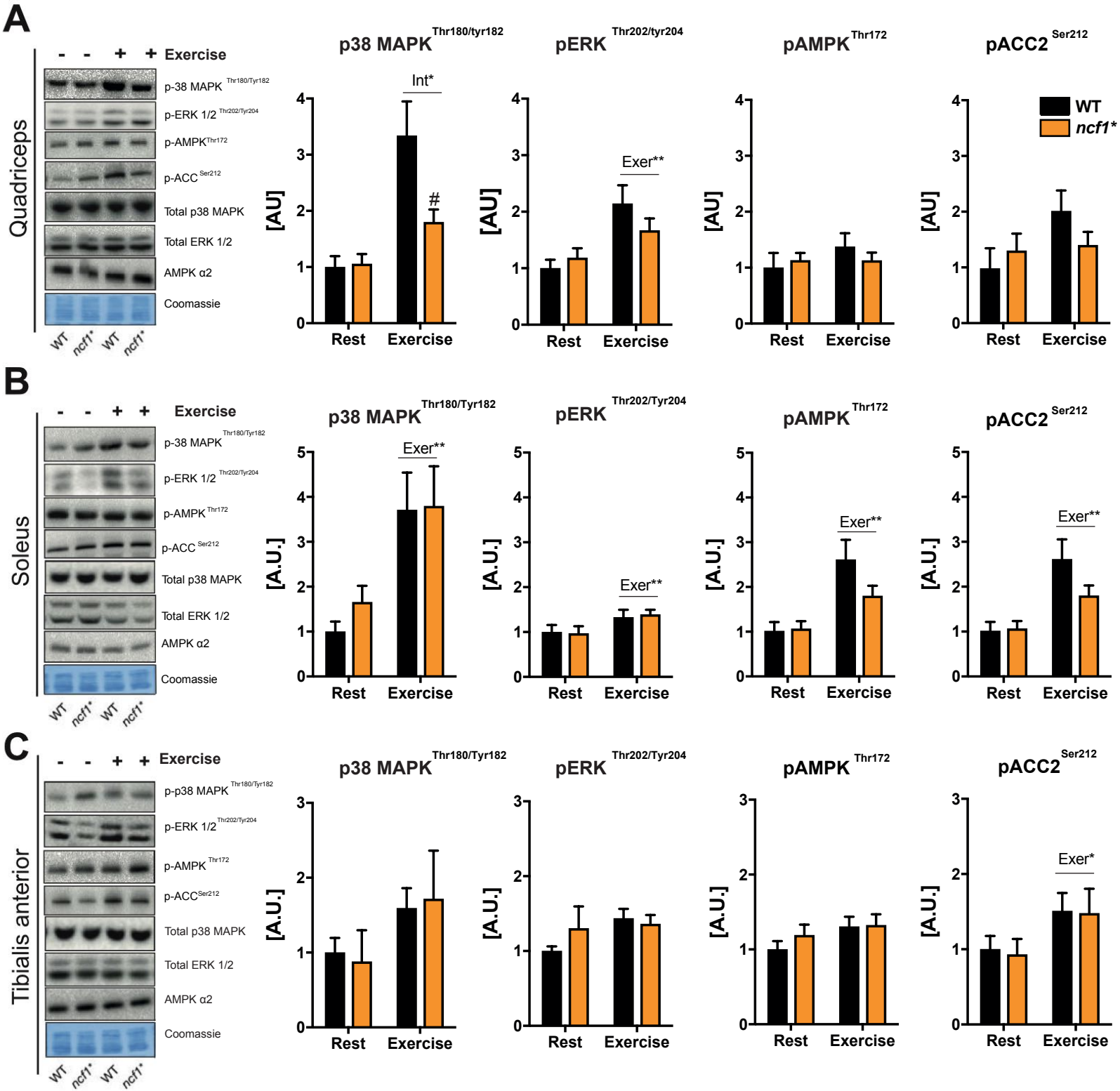
A
Quadriceps
- - + + Exercise
p-38 MAPK Thr180/Tyr182
p-ERK 1/2 Thr202/Tyr204
p-AMPK Thr172
p-ACC Ser212
Total p38 MAPK
Total ERK 1/2
AMPK α2
Coomassie
WT ncf1* WT ncf1*
p38 MAPK Thr180/tyr182
pERK Thr202/tyr204
pAMPK Thr172
pACC2 Ser212
WT
ncf1*
[AU]
Int*
#
Exer**
Rest
Exercise
B
Soleus
- - + + Exercise
p-38 MAPK Thr180/Tyr182
p-ERK 1/2 Thr202/Tyr204
p-AMPK Thr172
p-ACC Ser212
Total p38 MAPK
Total ERK 1/2
AMPK α2
Coomassie
WT ncf1* WT ncf1*
p38 MAPK Thr180/Tyr182
pERK Thr202/Tyr204
pAMPK Thr172
pACC2 Ser212
[A.U.]
Exer**
Rest
Exercise
C
Tibialis anterior
- - + + Exercise
p-p38 MAPK Thr180/Tyr182
p-ERK 1/2 Thr202/Tyr204
p-AMPK Thr172
p-ACC Ser212
Total p38 MAPK
Total ERK 1/2
AMPK α2
Coomassie
WT ncf1* WT ncf1*
p38 MAPK Thr180/Tyr182
pERK Thr202/Tyr204
pAMPK Thr172
pACC2 Ser212
[A.U.]
Exer*
Rest
Exercise

Figure S1

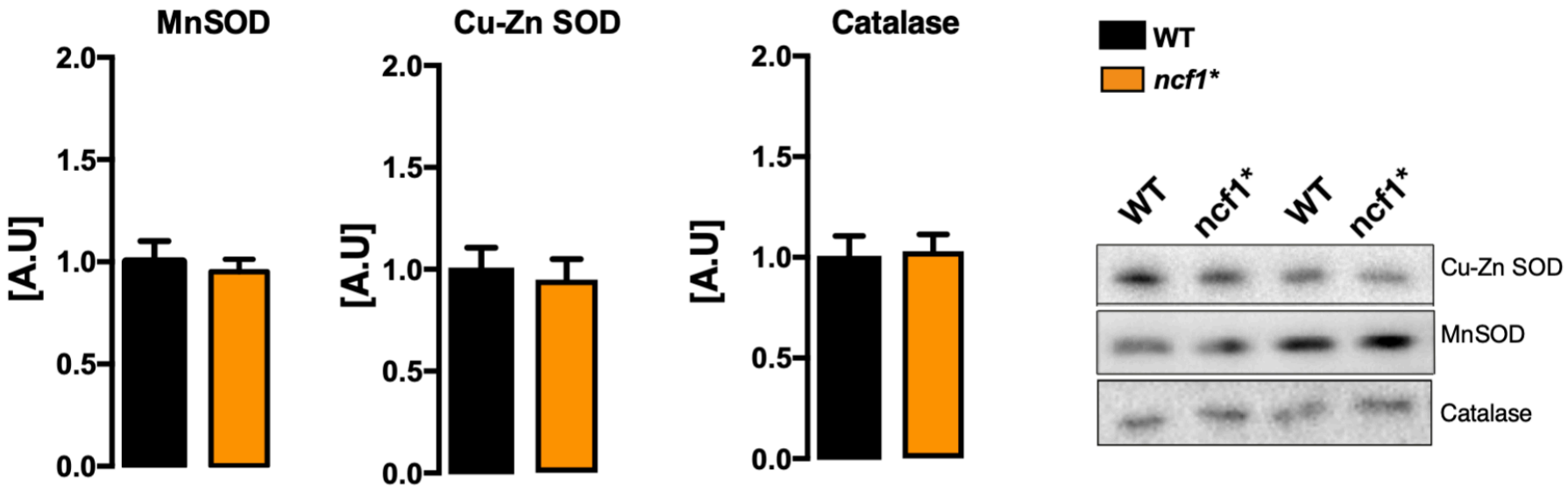
MnSOD
Cu-Zn SOD
Catalase
[A.U]
2.0
1.5
1.0
0.5
0.0
WT
ncf1*
WT
ncf1*
WT
ncf1*
Cu-Zn SOD
MnSOD
Catalase

Figure S2

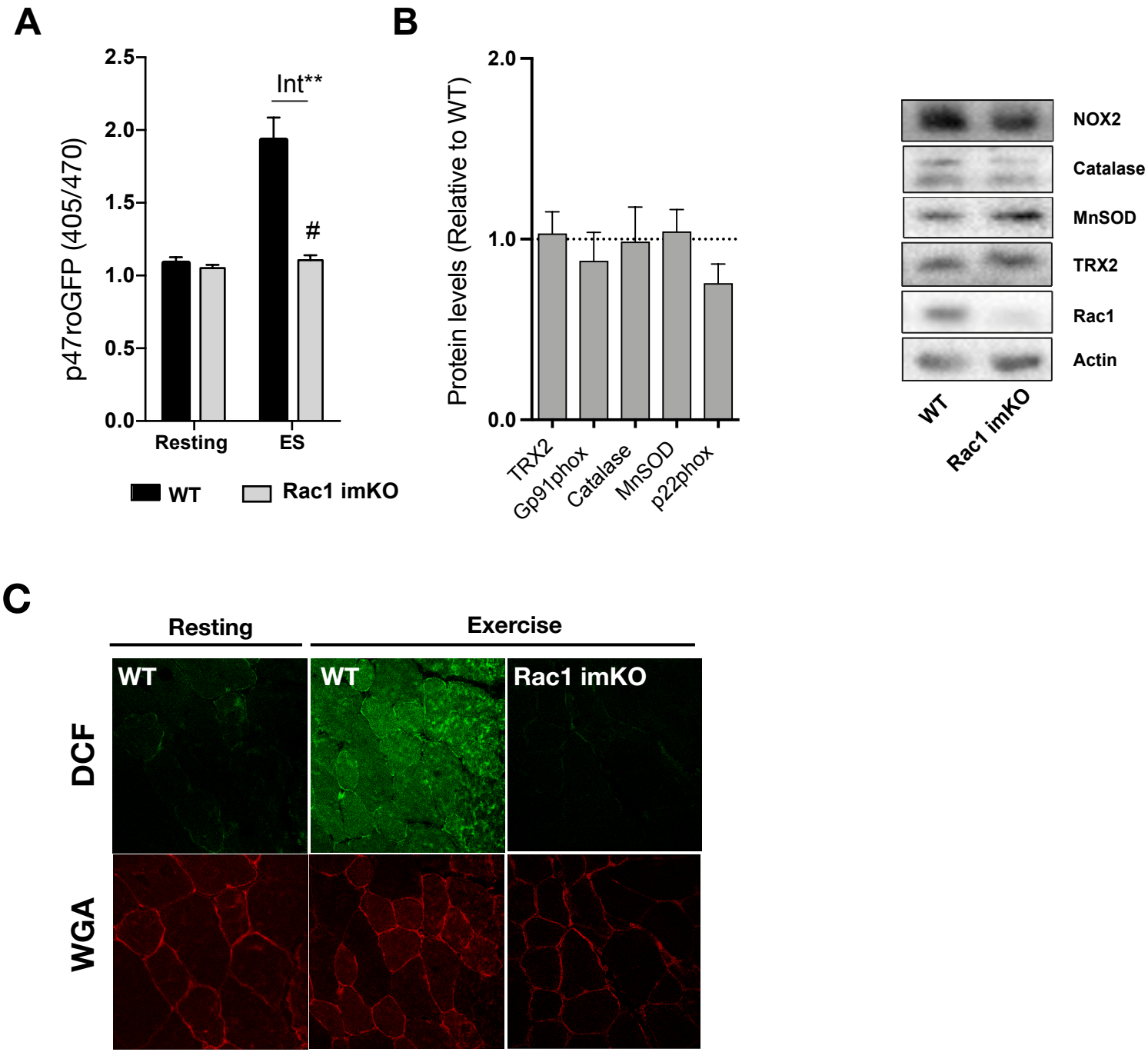
A
p47roGFP (405/470)
2.5
2.0
1.5
1.0
0.5
0.0
Int**
#
Resting
ES
WT
Rac1 imKO
B
Protein levels (Relative to WT)
2.0
1.0
0.0
TRX2
Gp91phox
Catalase
MnSOD
p22phox
NOX2
Catalase
MnSOD
TRX2
Rac1
Actin
WT
Rac1 imKO
C
Resting
Exercise
DCF
WGA
WT
WT
Rac1 imKO

Figure S3

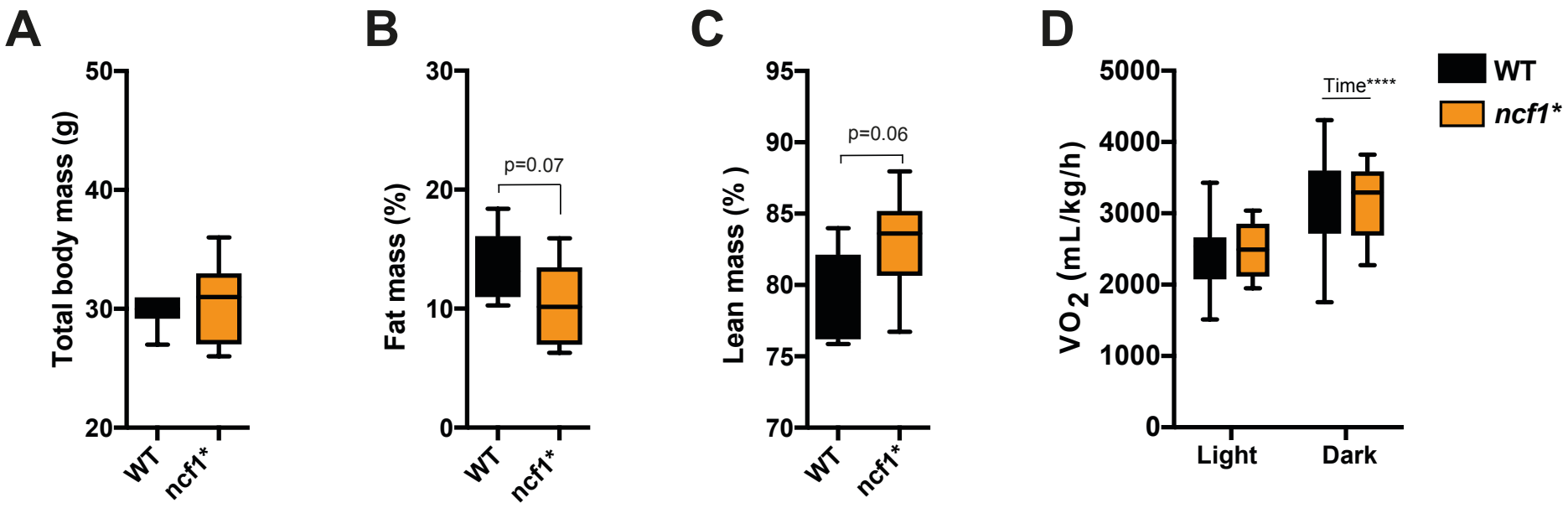
A
Total body mass (g)
50
40
30
20
WT
ncf1*
B
Fat mass (%)
30
20
10
0
p=0.07
WT
ncf1*
C
Lean mass (%)
95
90
85
80
75
70
p=0.06
WT
ncf1*
D
VO2 (mL/kg/h)
5000
4000
3000
2000
1000
0
Time****
Light
Dark
WT
ncf1*

Figure S4

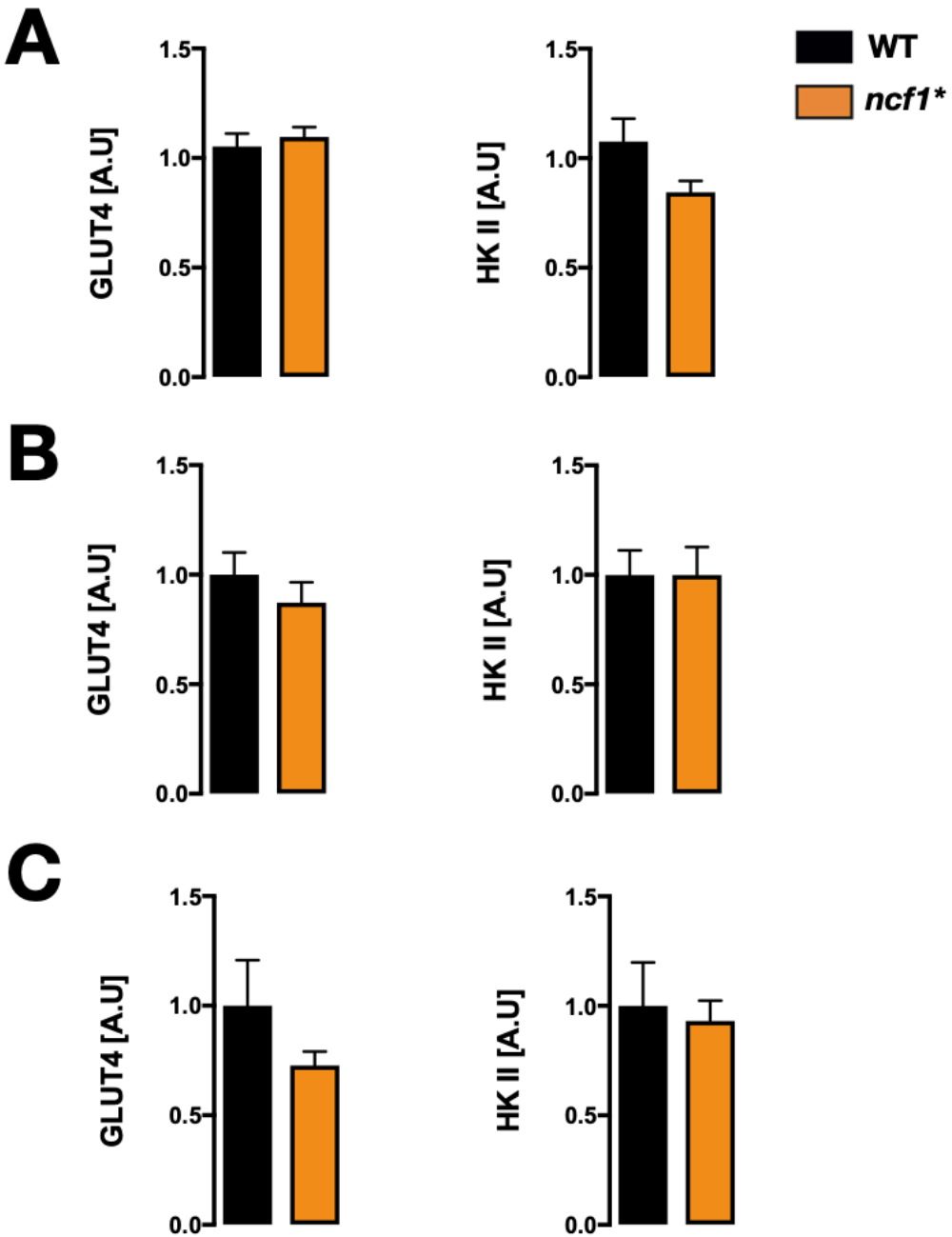

Figure S5

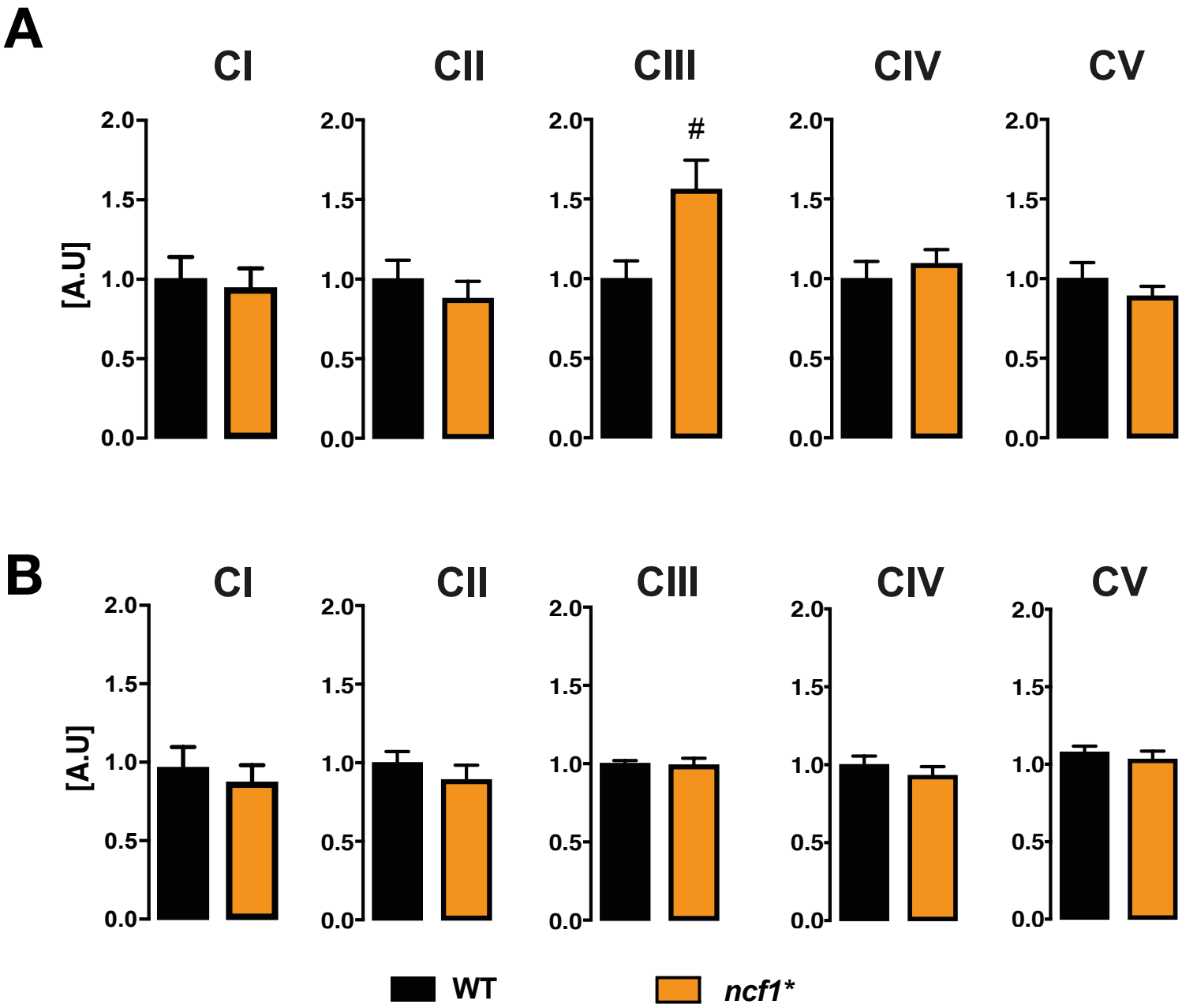
A
CI
CII
CIII
CIV
CV
[A.U]
2.0
1.5
1.0
0.5
0.0
#
B
CI
CII
CIII
CIV
CV
[A.U]
2.0
1.5
1.0
0.5
0.0
WT
ncf1*

Figure S6

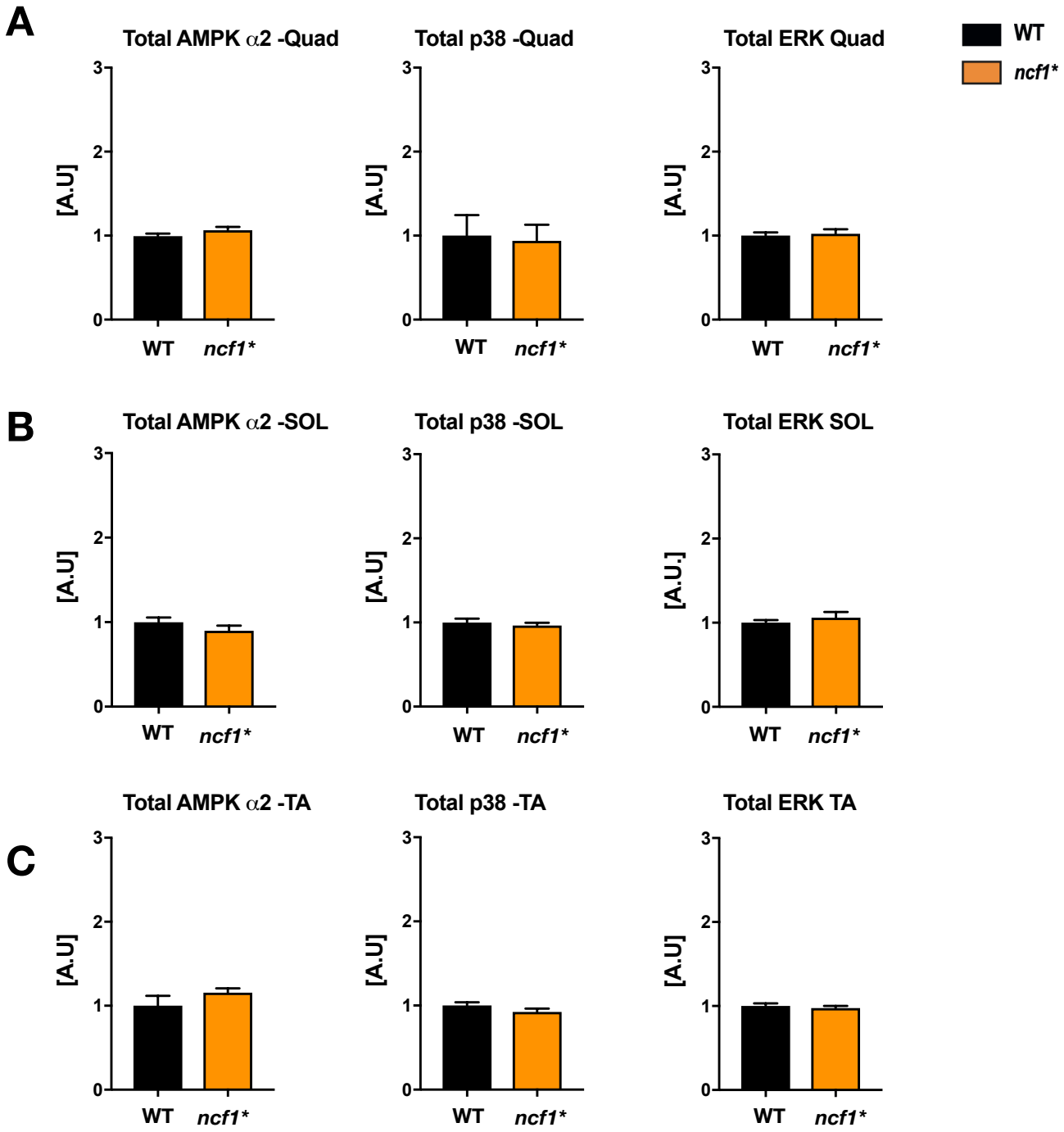
A
Total AMPK α2 -Quad
Total p38 -Quad
Total ERK Quad
WT
ncf1*
[A.U]
B
Total AMPK α2 -SOL
Total p38 -SOL
Total ERK SOL
[A.U.]
C
Total AMPK α2 -TA
Total p38 -TA
Total ERK TA
0
1
2
3